Fast Automatic Microstructural Segmentation of Ferrous Alloy Samples using Optimum-Path Forest

João Paulo Papa[1], Victor Hugo C. de Albuquerque[2], Alexandre Xavier Falcão[3], João Manuel R.S. Tavares[4]

[1] São Paulo State University, Computer Science Department, Bauru - Brazil
[2] University of Fortaleza, Technological Research Center, Fortaleza - Brazil
[3] University of Campinas, Institute of Computing, Campinas – Brazil
[4] University of Porto, Faculty of Engineering, Porto - Portugal

Abstract. In this work we propose a novel automatic cast iron segmentation approach based on the Optimum-Path Forest classifier (OPF). Microscopic images from nodular, gray and malleable cast irons are segmented using OPF, and Support Vector Machines (SVM) with Radial Basis Function and SVM without kernel mapping. Results show accurate and fast segmented images, in which OPF outperformed SVMs. Our work is the first into applying OPF for automatic cast iron segmentation.

Keywords: supervised classification, image segmentation, cast irons, microstructural evaluation, materials science.

1 Introduction

Cast irons are an iron-carbon-silicon alloy that have been used in numerous industrial applications, such as the base structures of manufacturing machines, rollers, valves, pump bodies and mechanical gears, among others. The main families of cast irons are: nodular cast iron, malleable cast iron, gray cast iron and white cast iron [3]. Their properties, as of all materials, are influenced by their microstructure and therefore, the correct characterization of their microstructure is highly important. Thus, metallographic evaluation of materials is commonly used to determine the quantity, appearance, size and distribution of the phases and constituents of materials. To carry this analysis, segmentation and quantification of the microstructure of cast irons from metallographic images is usually done.

Manual microstructural characterization, i.e., characterization based on human visual inspection, is an exhausting task, because the specialists spend much time exposed to high luminosities in the microscope device, which can produce fatigue and, consequently, increase the probability of measurement errors.

Several works for automatic microstructural image analysis have been developed based on computer vision techniques [2,6,11,15]. Scozzafava et al. [15] presented an approach for graphite nodules shape characterization, in which spheroidal cast irons were evaluated aiming to obtain quantitative analysis of their constitutive elements.

Images of the metallographic sections acquired by means of a light optical microscope were processed in order to obtain a simpler image representation, in which the nodules are black regions over a white background, and a method for automatic classification of the graphite's shape particles in cast iron was proposed by De Santis et al. [6]. Shape and size parameters for discriminating cast iron are commonly used features, but Gomes et al. [9] have proposed a new parameter, the average internal angle, and shown its relevance for accurate classification. However, such techniques consider image segmentation based on global threshold binarization, which are frequently defined by manual adjustment in function of the image to be analyzed, or even so in local measurements. These approaches are proponed to errors, mainly because of the amount of the noise in the images to be analyzed.

Other works are based on artificial intelligence for the evaluation of cast iron microstructures. Jiang et al. [11] used six types of gray cast iron and an Artificial Neural Network (ANN) [6] for their categorization. Zhibin et al. [17] have presented a nodular cast iron recognition system based on fuzzy approach. Albuquerque et al. [1, 2] addressed the segmentation and quantification of the cast iron microstructures obtained from metallographic images by means of an ANN using multilayer perceptron (ANN-MLP) and Self-Organizing Maps (SOM) [6]. However, as an unstable classifier, collections of ANN-MLP can improve its performance up to some unknown limit of classifiers [10]. SOM networks suffer from the high computational burden, in which its parameters choice, i. e., neural network architecture, is a hard task, and strongly depends on each application. Artificial neural networks with Radial Basis Function (RBF) also have their limitations. Different from ANN-MLP, which find hyperplanes to separate elements from different classes, ANN-RBF make use of hyperellipsoids to best cluster data into groups [6]. The main problem relies on the parameters that need to be estimated for these geometrical polygons, i. e., the hyperellipsoids' center and standard deviation.

Support Vector Machines (SVM) is another pattern recognition technique that have been extremely used in several applications, which assume linearly separable classes in a higher-dimensional feature space [5]. However, its computational cost rapidly increases with the training set size and the number of support vectors. As a binary classifier, multiple SVM are required to solve a multi-class problem. Tang and Mazzoni [16] proposed a method to reduce the number of support vectors in the multi-class problem. Their approach suffers from slow convergence and high computational cost, because they first minimize the number of support vectors in several binary SVM, and then share these vectors among the machines. However, in all SVM approaches, the assumption of separability may also not be valid in any space of finite dimension [14].

Therefore, the commonly used pattern recognition techniques cannot handle both efficiency and effectiveness in the overall process, i.e., training and test phases. Another question that needed to be pointed out is that there is a need for fast automatic cast iron microstructures identification given that, usually, the metallographic images are obtained from high-resolution sensors, which generate images with millions of pixels. This context makes unviable the use of artificial neural networks and SVM due to their high computational burden in the training phase. Although the training step can be performed in a separated manner, such techniques cannot handle real time and iterative segmentation systems for cast iron microstructures. Imagine that you have a system in which the technician can mark some samples from each kind of cast iron in a given high resolution image. After that, the system needs to be trained in order to classify the

remaining image pixels. After that, the user can modify the classified image in order to make this process more accurate, marking some misclassified pixels with their correct labels. In this context, the system needs to be retrained for further classification. This overall process can be executed until some criteria (e.g., the user compliance with the final result). As aforementioned, a simple selection of some pixels by user in such kind of images can involve several hundreds of pixels. In such a way, it is reasonable to assume that the user can wait for a just few seconds for the cast iron microstructures classification.

Recently, a novel graph-based classifier that reduce the pattern recognition problem as an optimum-path forest (OPF) computation in the feature space induced by a graph was presented [12]. The OPF classifier does not interprets the classification task as a hyperplanes optimization problem, but as a polynomial combinatorial optimum-path computation from some key samples (prototypes) to the remaining nodes. Each prototype becomes a root from its optimum-path tree and each node is classified according to its strongly connected prototype. This process defines a discrete optimal partition (influence region) of the feature space. The OPF classifier has some advantages with respect to the aforementioned classifiers: (i) is free of parameters, (ii) do not assume any shape/separability of the feature space, (iii) run training phase faster and (iv) make decisions based on a global criteria. Results in several applications, such that fingerprint and face recognition, remote sensing image classification, biomedical signal processing and many other works, have been demonstrated that OPF is superior than ANN-MLP, SOM and k-Nearest Neighbors (k-NN), and similar to SVM, but much faster [12].

This paper presents an innovative computational tool based on OPF classifier for the analysis of images of ferrous alloys, which optimizes the process of segmentation and quantification of their microstructures. We are the first into applying the optimum-path forest classifier in this research field, usually called by quantitative metallography. In order to accomplish comparisons about computational cost, accuracy, and speed in the segmentation and quantification process with other classifiers, images from nodular, gray and malleable cast irons were analyzed using OPF and SVM using Radial Basis Function kernel and SVM without kernel mapping. Additionally, visual and analytical comparisons were also addressed. This paper is organized as follows. The next section presented the OPF classifier theory. Section 3 discusses the experimental results. Finally, the Section 4 states conclusions and future works.

2 Optimum-Path Forest Classifier

Let Z_1 and Z_2 be training and test sets with $|Z_1|$ and $|Z_2|$ samples of a given dataset. Here, we use samples as pixels of images. Let $\lambda(s)$ be the function that assigns the correct label i, $i = 1,2,\ldots,c$, to any sample $s \in Z_1 \cup Z_2$, $S \subseteq Z_1$ be a set of prototypes from all classes, and v be an algorithm that extracts n features (Red, Blue and Green values from each pixel) from any sample $s \in Z_1 \cup Z_2$ and

returns a vector $\vec{v}(s)$. The distance $d(s,t) > 0$ between two samples, s and t, is the one between their corresponding feature vectors $\vec{v}(s)$ and $\vec{v}(t)$. One can use any distance function suitable for the extracted features, been the most common the Euclidean norm [12].

Our problem consists of projecting a classifier that can predict the correct label $\lambda(s)$ of any sample $s \in Z_2$. Training consists of finding a special set $S^* \subseteq Z_1$ of prototypes and a discrete optimal partition of Z_1 in the feature space (i.e., an optimum-path forest rooted in S^*). The classification of a sample $s \in Z_2$ is done by evaluating the optimum paths incrementally, as though it were part of the forest, and assigning to it the label of the most strongly connected prototype.

2.1 Training

Let (Z_1, A) be a complete graph whose nodes are the training samples and any pair of samples defines an arc in $A = Z_1 x Z_1$ (Fig. 1a). The arcs do not need to be stored and so the graph does not need to be explicitly represented. A path is a sequence of distinct samples $\pi_t = \langle s_1, s_2, \ldots, t \rangle$ with terminus at a sample t. A path is said trivial if $\pi_t = \langle t \rangle$. We assign to each path π_t a cost $f(\pi_t)$ given by a connectivity function f. A path π_t is said optimum if $f(\pi_t) \leq f(\pi_\tau)$ for any other path π_τ. We also denote by $\pi_s \cdot \langle s,t \rangle$ the concatenation of a path π_s and an arc (s,t).

We will address the connectivity function $f_{\max}$:

$$\begin{aligned} f_{\max}(\langle s \rangle) &= \begin{cases} 0 \ if \ s \in S \\ +\infty \ otherwise, \end{cases} \\ f_{\max}(\pi_s \cdot \langle s,t \rangle) &= \max\{f_{\max}(\pi_s), d(s,t)\}, \end{aligned} \tag{1}$$

such that $f_{\max}(\pi_s \cdot \langle s,t \rangle)$ computes the maximum distance between adjacent samples along the path $\pi_s \cdot \langle s,t \rangle$. The minimization of $f_{\max}$ assigns to every sample $t \in Z_1$ an optimum path $P^*(t)$ from the set $S \in Z_1$ of prototypes, whose minimum cost $C(t)$ is:

$$C(t) = \min_{\forall \pi_t \in (Z_1, A)} \{f_{\max}(\pi_t)\}. \tag{2}$$

The minimization of $f_{\max}$ is computed by *Algorithm 1*, called OPF algorithm, which is an extension of the general image foresting transform (IFT) algorithm [7] from the image domain to the feature space, here specialized for $f_{\max}$. This process assigns one optimum path from S to each training sample t in a non-decreasing order of minimum cost, such that the graph is partitioned into an optimum-path forest P (a function with no cycles which assigns to each $t \in Z_1 \setminus S$ its predecessor $P(t)$ in $P^*(t)$ or a marker nil when $t \in S$, as shown in Fig. 1b). The root $R(t) \in S$ of $P^*(t)$ can be obtained from $P(t)$ by following the predecessors backwards along the path, but its label is propagated during the algorithm by setting $L(t) = \lambda(R(t))$.

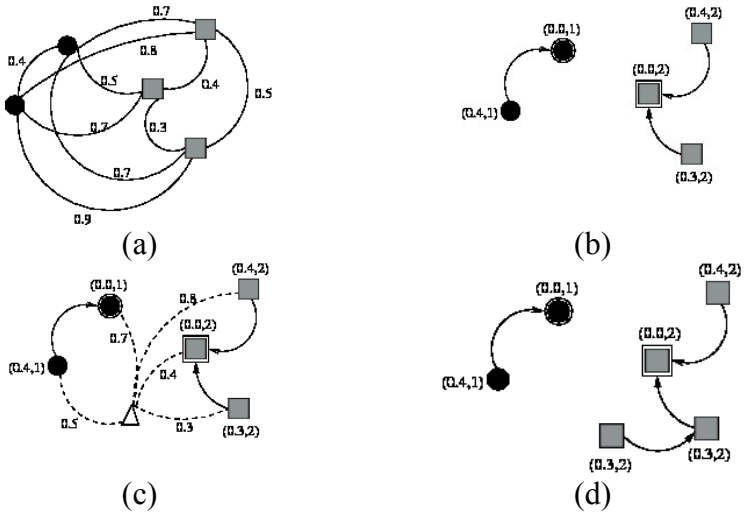

Fig. 1. (a) Complete weighted graph for a simple training set. (b) Resulting optimum-path forest for $f_{\max}$ and two given prototypes (circled nodes). The entries (x, y) over the nodes are, respectively, the cost and the label of the samples. The directed arcs indicate the predecessor nodes in the optimum path. (c) Test sample (white triangle) and its connections (dashed lines) with the training nodes. (d) The optimum path from the most strongly connected prototype, its label *2*, and classification cost *0.3* are assigned to the test sample.

Follow, bellow, the OPF classifier algorithm. Lines 1-3 initialize maps and insert prototypes in Q. The main loop computes an optimum path from S to every sample s in a non-decreasing order of minimum cost (Lines 4-11). At each iteration, a path of minimum cost $C(s)$ is obtained in P when we remove its last node s from Q (Line 5). Ties are broken in Q using first-in-first-out policy. That is, when two optimum paths reach an ambiguous sample s with the same minimum cost, s is

assigned to the first path that reached it. Note that $C(t) > C(s)$ in Line 6 is false when t has been removed from Q and, therefore, $C(t) \neq \infty$ in Line 9 is true only when $t \in Q$. Lines 8-11 evaluate if the path that reaches an adjacent node t through s has a cost lower than the current path with terminus t and update the position of t in Q, $C(t)$, $L(t)$ and $P(t)$ accordingly.

OPF Algorithm

Input: A training set Z_1, λ-labeled prototypes $S \subseteq Z_1$ and the pair (v, d) for feature vector and distance computations.
Output: Optimum-path forest P, cost map C and label map L.
Auxiliary: Priority queue Q and cost variable cst.

1. For each $s \in Z_1 \setminus S$, set $C(s) = +\infty$.
2. For each $s \in S$, do
  2.1. $C(s) = 0$, $P(s) = nil$, $L(s) = \lambda(s)$, and insert s in Q.
3. While Q is not empty, do
  3.1. Remove from Q a sample s such that $C(s)$ is minimum.
  3.2. For each $t \in Z_1$ such that $t \neq s$ and $C(t) > C(s)$, do
    3.2.1. Compute $cst = \max\{C(s), d(s,t)\}$.
    3.2.2. If $cst < C(t)$, then
      3.2.2.1. If $C(t) \neq +\infty$, then remove t from Q.
      3.2.2.2. $P(t) = s$, $L(t) = L(s)$ and $C(t) = cst$.
      3.2.2.3. Insert t in Q.

2.2 Classification

For any sample $t \in Z_2$, one consider all arcs connecting t with samples $s \in Z_1$, as though t were part of the training graph (Fig. 1c). Considering all possible paths from S^* to t, one find the optimum path $P^*(t)$ from S^* and label t with the class $\lambda(R(t))$ of its most strongly connected prototype $R(t) \in S^*$. This path can be identified incrementally, by evaluating the optimum cost $C(t)$ as:

$$C(t) = \min_{\forall s \in Z_1} \{\max\{C(s), d(s,t)\}\}. \quad (3)$$

Let the node $s^* \in Z_1$ be the one that satisfies Equation 3 (i.e., the predecessor $P(t)$ in the optimum path $P^*(t)$). Given that $L(s^*) = \lambda(R(t))$, the classification simply assigns $L(s^*)$ as the class of t (Fig. 1d). An error occurs when $L(s^*) \neq \lambda(t)$.

3 Experimental Results

In this section we will describe the dataset used, as well as the evaluation methodology for the microstructural characterization of the computational methods used.

3.1 Dataset

For the application of the computational methods used here, it was necessary to perform, firstly, the metallographic preparation of the cast iron samples to be analyzed. Then, the samples were microscopically analyzed, accomplishing with a brightness and contrast adjustment, and acquired the correspondent images. Fig. 2 displays some examples of the cast iron images used.

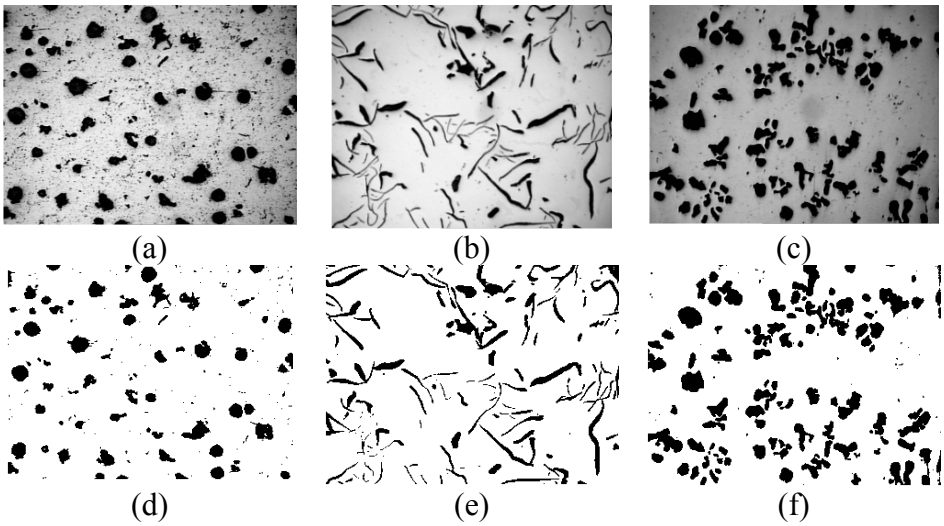

Fig. 2. Microstructure images of cast irons: (a) nodular, (b) gray and (c) malleable and their respective labeled images in (d), (e) and (f). All images shown in this paper have 320x240 pixels and, for visualization purposes, a magnification of 100x was applied on them.

3.2 Classifiers

We evaluated the cast iron segmentation by means of three supervised classifiers: Support Vector Machines using Radial Basis Function (SVM-RBF) for kernel mapping, Support Vector Machines without kernel mapping (SVM-LINEAR), and Optimum-Path Forest (OPF). We used as features, for each pixel, its RGB values.

For SVM-RBF, we used the latest version of the LibSVM package [4] with Radial Basis Function (RBF) kernel, parameter optimization and the one-versus-one strategy for the multi-class problem. With respect to SVM-LINEAR, we used the LibLINEAR package [8] with C parameter optimized using cross validation. Regarding OPF we used the LibOPF [13], which is a library for the design of optimum-path forest-based classifiers

3.3 Results from Experiments

We performed two series of experiments: in the former (Section 3.3.1) we used one image from each cast iron type (nodular, gray, and malleable in Fig. 2) to evaluate the effectiveness of the classifiers. For training classifiers, we used 1% of the whole image and the remaining 99% for testing, and in the last experiment (Section 3.3.2) we used the classifiers trained in previous images to segment new ones (Fig. 3).

3.3.1 Robustness of the Classifiers

We used 1% (768 samples) of the whole image (one for each cast iron) for training classifiers and 99% (69120 samples) to test them (the images were labeled by a technician – see Figures 2d, 2e and 2f). Notice that here the SVM-RBF, SVM-LINEAR, and OPF algorithms were executed 10 times with randomly generated training and test sets, to compute the mean accuracy and its standard deviation, and the mean training and test execution times in seconds. The accuracy was computed by taking into account that the classes may have different sizes using a methodology proposed by Papa et al. [12]. Tables 1, 2 and 3 display the results for the different cast irons.

Table 1. Evaluation of the classifiers into classifying nodular cast iron with respect to the mean accuracy and mean execution times.

Classifier	Mean accuracy	Mean training execution time [s]	Mean test execution time [s]
OPF	**96.26 % ± 5.58**	**0.478548**	**4.097354**
SVM-RBF	73.75 % ± 23.94	124.929431	2.029066
SVM-LINEAR	81.16 % ± 22.64	114.229541	0.055253

Segmentation of Ferrous Alloy Samples

Table 2. Evaluation of the classifiers into classifying gray cast iron with respect to the mean accuracy and mean execution times.

Classifier	Mean accuracy	Mean training execution time [s]	Mean test execution time [s]
OPF	**99.83 % ± 0.24**	**0.048117**	**5.434169**
SVM-RBF	99.62 % ± 0.32	23.883542	1.746221
SVM-LINEAR	93.70 % ± 3.68	24.924486	0.163015

Table 3. Evaluation of the classifiers into classifying malleable cast iron with respect to the mean accuracy and mean execution times.

Classifier	Mean accuracy	Mean training execution time [s]	Mean test execution time [s]
OPF	**99.86 % ± 0.19**	**0.051487**	**5.737038**
SVM-RBF	99.59 % ± 0.37	20.336996	1.059828
SVM-LINEAR	98.69 % ± 0.83	10.927093	0.163563

From Tables 1, 2 and 3, we can see that OPF classifier outperformed SVM-RBF, and SVM-LINEAR for nodular cast iron. Although the results were similar for gray and malleable cast iron, OPF was 497.5 times and 392.68 times faster than SVM-RBF in the training phase for gray and malleable cast iron, respectively. Finally, for malleable cast iron, OPF and SVM-RBF achieved similar results, being OPF and SVM-LINEAR faster in the training and test phases, respectively.

3.3.2 Cast Iron Segmentation Analysis

In this section we show the experiment results for automatic cast iron segmentation. We used 1% of the images used in the previous experiment (Fig. 2), from each cast iron, to train the classifiers. Further, we evaluated them in another collection of images, whose segmentation results are displayed in Fig. 3.

The results appear to be similar for all cast iron images, in which the classifiers performed good segmentation results. For gray cast iron, one can see that SVM_RBF and SVM-LINEAR methods lose some graphite particles (see the top left region of Fig. 3b, 3e, 3h and 3k), which modify completely the results of quantification of microstructure of the samples used. However, when we used the OPF classifier these particles are totally preserved. Thus, regarding SVM classifiers, this method presents better segmentation results, is faster, is lesser computational demanded, and principally more accurate.

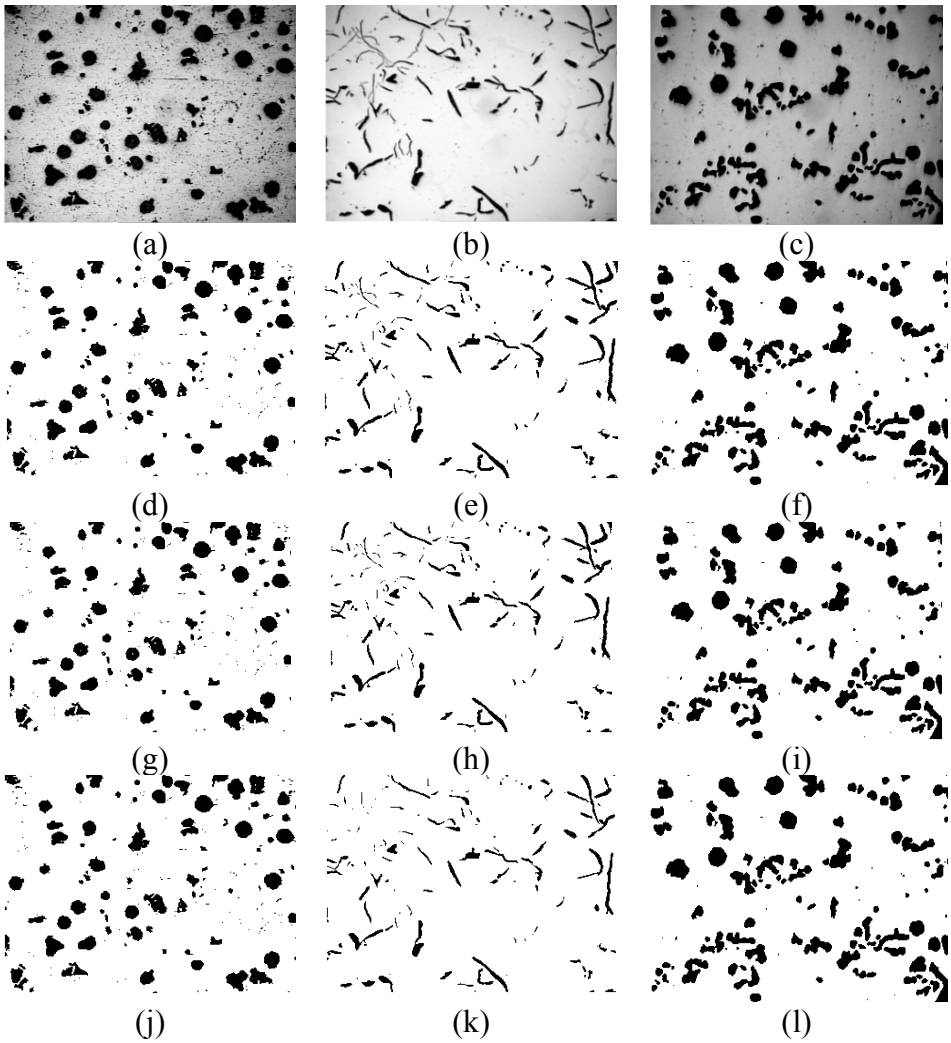

Fig. 3. Original cast iron images: (a) nodular, (b) gray, and (c) malleable; OPF segmentation results in (d)-(f), SVM-RBF results in (g)-(i) and, finally, SVM-LINEAR segmentation ones in (j)-(l).

4 Conclusions

We have presented a new methodology for fast automatic cast iron segmentation using the Optimum-Path Forest classifier, which is characterized by its extremely efficiency allied with goof effectiveness.

In the experimental evaluation we performed two rounds of experiments. In the former, we compared OPF against SVM-RBF and SVM-LINEAR by using 1% of the

input image for training and the remaining 99% for testing. The OPF outperformed SVM-RBF and SVM-LINEAR in both efficiency (overall execution time, i.e., training + testing) and effectiveness. Only for the malleable cast iron that the classifiers achieved similar results. In the last round of experiments, we used the classifiers trained in the previous one to segment another collection of cast iron images. The classifiers achieved similar segmentation results, except for the gray cast iron, in which the OPF segmented successfully more structures than SVM-RBF and SVM-LINEAR. With the work reported, we are the first ones into applying the OPF classifier for cast iron image segmentation, and also in the microstructural analysis of microstructures of metallic materials.

For future works, we are interested into segment white cast irons, as well as on comparing the methods here considered with others computational techniques as Artificial Neural Network using multilayer perceptron (ANN-MLP), and self-organized maps (ANN-SOM) training algorithms.

Acknowledgments

This work was partially done in the scope of the project with reference PTDC/EEA-CRO/103320/2008, financially supported by FCT – Fundação para Ciência e Tecnologia of Portugal.

References

1. Albuquerque V.H.C., Alexandria A.R., Cortez P.C., Tavares J.M.R.S.: Evaluation of multilayer perceptron and self-organizing map neural network topologies applied on microstructure segmentation from metallographic images. NDT & E International, vol. 42, no. 7, 644--651 (2009)
2. Albuquerque V.H.C., Cortez P.C., Alexandria A.R., Tavares J.M.R.S.: A new solution for automatic microstructures analysis from images based on a backpropagation artificial neural network. Non-destructive Testing and Evaluation, vol. 23, no. 4, 273--283 (2008)
3. Callister, W.D.: Materials science and engineering: an introduction. New York, John Wiley & Sons Inc (2006)
4. Chang C. C., Lin C. J.: LIBSVM: A Library for Support Vector Machines. Software available at http://www.csie.ntu.edu.tw/~cjlin/libSVM (2001)
5. Cortes C., Vapnik V.: Support-Vector Networks. Machine Learning, vol. 20, no. 3, 273 -- 297 (1995)
6. De Santis A., Di Bartolomeo O., Iacoviello D., Iacoviello F.: Quantitative shape evaluation of graphite particles in ductile iron. Journal of Materials Processing Technology, vol. 196, 292--302 (2008)
7. Falcão A.X., Stolfi J., Lotufo R.A.: The Image Foresting Transform: Theory, Algorithm and Applications. IEEE Transactions on Pattern Analysis and Machine Intelligence, vol. 26, no. 1, 19--29 (2004)
8. Fan R.-E., Chang K.-W., Hsieh C.-J., Wang X.-R., Lin C.-J.: LIBLINEAR: A Library for Large Linear Classification. Journal of Machine Learning Research, vol. 9, 1871—1874 (2008)

9. Gomes O. F.M., Paciornik S.: Automatic Classification of Graphite in Cast Iron. Microscopy and Microanalysis, vol. 11, 363--371 (2005)
10. Haykin S.: Neural Networks: A comprehensive foundation. Prentice-Hall (1998)
11. Jiang H., Tan Y., Lei J., Zeng L, Zhang Z. and Hu1 J.: Auto-analysis system for graphite morphology of grey cast iron. Journal of Automated Methods & Management in Chemistry, vol. 25, no. 4, 87-- 92 (2003)
12. Papa J.P., Falcão A.X., Suzuki C.T.N.: Supervised Pattern Classification based on Optimum-Path Forest. International. Journal of Imaging Systems and Technology, vol. 19, no. 2, 120--131 (2009)
13. Papa J.P., Suzuki C.T.N., Falcão A.X.: LibOPF: A library for the design of optimum-path forest classifiers. Software available at http://www.ic.unicamp.br/~afalcao/LibOPF (2008)
14. Reyzin L., Schapire R.E.: How Boosting the Margin Can Also Boost Classifier Complexity. In: Proceedings of the 23rd International Conference on Machine Learning, vol. 8, 753--760 (2006)
15. Scozzafava A., Tomesani L., Zucchelli A.: Image analysis automation of spheroidal cast iron. Journal of Materials Processing Technology, vol. 153-154, 853--859 (2004)
16. Tang B., Mazzoni D.: Multiclass Reduced-set Support Vector Machines. In: Proceedings of the 23rd International Conference on Machine Learning, 921--928 (2006)
17. Zhibin C., Yongquan Y., Heqing C., Shaomin Y.: Fuzzy recognition of graphite morphology in nodular cast iron based on evolution strategy. In: Proceedings of 2005 International Conference on Machine Learning and Cybernetics, vol. 8, 4930--4935 (2005)